# Robust Sharpness Metrics using Reorganized DCT Coefficients for Auto-Focus Application

Zheng Zhang, Yu Liu, Xin Tan, Maojun Zhang

College of Information System and Management
National University of Defense Technology
Changsha, Hunan, P.R. China, 410073

**Abstract.** We present two new metrics for measuring sharpness of an image. Both methods exploit a reorganized Discrete Cosine Transform (DCT) representation and analyze the reorganized coefficients to use the most useful components for sharpness measuring. Our first metric utilizes optimal high and middle frequency coefficients for relative sharpness evaluation. It is well suitable for focus measure as it is super sensitive to the best-focus position and could predict stable and accurate focus values for various subjects and scenes with different lighting and noise conditions. Experiments demonstrate that it has high discrimination power even for high noisy and low-contrast images. The second metric constructs energy maps for each scale of reorganized DCT coefficients, and determines absolute sharpness/blurriness using the local maxima energy information. Compared with most existing no-reference sharpness/blurriness metrics, this metric is very efficient in sharpness measurement for images with different contents, and can be used in real-time auto-focus application. Experiments show that it correlates well with perceived sharpness.

## 1 Introduction

The perceptions of sharpness and blurriness are closely related to the details and clarity of an image. Most often they are used as antonyms since sharpness is inversely proportional to blurriness. For sharpness or blurriness measurement, subjective method that relies on human observations is accurate but has limited use for imaging applications. By contrast, objective metric which automatically assesses the degree of sharpness/blurriness is important for many applications of image processing and computer vision. One important application of sharpness measurement is for contrast-based auto-focus. In contrast-based auto-focus, a measure of focus is detected from each image acquired at different lens positions, and is used for adjusting the camera lens to locate the in-focus position by finding the maximum focus measure. Focus measure is normally defined in terms of sharpness, which is computed by a sharpness metric. Because the maximum focus measure corresponds to the best focused position, the sharpness metric largely determines focusing accuracy. Other important applications of sharpness measurement include image quality assessment, image enhancement and restoration, for all of which the sharpness evaluation may play critical roles in the design and optimization of the relevant algorithms.

The accurate evaluation of image sharpness is a difficult problem because sharpness is affected by many factors such as the image content, illumination, noise and spatial activity [1, 2]. Our motivation of developing new sharpness metrics is twofold. Firstly, we are interested in accurate and robust relative sharpness measures. A relative sharpness metric is designed to predict sharpness of images that have the same content but may fail for different images. It is often used as a focus measure for auto-focus systems where the relative largest sharpness point determines the best-focus position. For actual autofocusing, the subjects being focused vary across scenes, being static or dynamic, having strong or poor contrast, with different illumination conditions that may cause serious noisy distortion and poor image quality. Although various relative sharpness metrics for focus measurement have been proposed [3–10], seldom methods are reported to be suitable for autofocusing in different scenes under severe illumination conditions. We are motivated to design a new relative sharpness metric that is robust to noise, illuminations, scene movements and low-contrast image contents. Secondly, we are also interested in evaluating an absolute value of sharpness for an given image. An absolute sharpness measure means its evaluation is not relative to a reference image, *i.e.*, it is a no-reference sharpness measure. It can discriminate the degree of sharpness among images that have different contents. Existing no-reference sharpness metrics are oriented to estimate extra parameters [11, 12, 2, 13, 1], and tend to have high computation complexity. These methods may produce accurate estimations but may not be suitable for situations where limited computation resource is available and real-time performance is needed. For our purpose, we desire a simple and efficient absolute sharpness metric which would be used combined with the relative sharpness metric for efficient autofocusing.

In this work, we first propose a robust DCT-based relative sharpness metric, where we exploit reorganized DCT coefficients to select the most suitable components that have high effect on sharpness measure. A nice property of our metric is that it has high discrimination power even for high noisy and low-contrast images.It is very suitable for focus measure as it is super sensitive to the best-focus position and could predict stable and accurate focus values for various subjects and scenes with different lighting and noise conditions. We also present an efficient DCT-based absolute sharpness metric. This metric exploits the same framework of the reorganized DCT representation. It correlates well with perceived sharpness and is efficient in sharpness measurement for images with different contents. We demonstrate the performance of our metrics by comparing them against several most commonly used metrics both on public Gaussian blur images of the LIVE dataset [14] and the captured out-of-focus sequences.

## 2 Related Work

Many sharpness metrics are developed mainly for the application of auto-focus, where these metrics are used to give a relative evaluation of sharpness for measuring focus. Because an auto-focus system generally requires real-time performance for various scenes under different illumination conditions, these rel-

ative sharpness metrics are required to be robust and efficient. Existing spatial-domain relative sharpness metrics [3, 15, 4] often determine sharpness by exploiting edge, gray scale, histogram or correlation information, while frequency-domain methods [16, 17, 8, 6, 7, 9] first transform image to a frequency domain using the fast Fourier transform (FFT) [18], DCT [8, 6, 7, 9] or discrete wavelet transform (DWT) [16, 17], and then compute sharpness with the high or middle frequency components of the transformed data. Generally, spatial-domain sharpness measures are relative computational efficiency, but mostly sensitive to noise [19, 20]. This would cause many local maxima in focus curve especially for scenes under low illumination conditions, making it difficult for autofocusing to find the best focused position. Frequency-domain methods usually require more computational cost as they need an extra frequency transform step. Because they calculate sharpness based on selecting of desired high or middle frequency coefficients, they are relatively insensitive to noise [20, 5].

Besides these relative sharpness metrics, there are also many no-reference metrics that are designed for absolute sharpness evaluation. In theory, an absolute sharpness metric can give an absolute evaluation of image sharpness regardless of the image contents. One typical way is to exploit the information of edges [21–23]. The method of [21] first detects edges of an image and then evaluate the blurriness based on the edge widths. The work [22] presents two blurriness metrics that are based on an analysis of the edges and adjacent regions in an image. In [23], the authors present the notion of just noticeable blur (JNB) and integrate it into a probability summation model. The work [24] improves the method of [12] by incorporating a visual attention model. Similarly, [23] also uses the concept of JNB and combines it with the cumulative probability of detecting blur at an edge. There are also spatial algorithms that do not rely on measuring the spread of edges. For example, the method of [25] utilizes eigenvalues of an image to evaluate sharpness.

Various frequency methods are also proposed for absolute sharpness/blurriness estimation. The work [26] computes sharpness using the average 2D kurtosis of the $8 \times 8$ DCT blocks. The work [11] presents a blurriness metric that is based on histogram computation of non-zero DCT coefficients. The method [27] uses Harr wavelet transform for sharpness analysis. In [28], a sharpness metric that uses both frequency contents and spatial features in one framework in order to avoid the pitfalls of alternative methods. The work [2] also utilizes both spectral and spatial features of an image, where the magnitude spectrum and the total spatial variation is measured for sharpness evaluation.

## 3 The Proposed Relative Sharpness Metric

We propose a relative sharpness metric that is designed for sharpness evaluation of images having similar scenes. This metric is suitable for auto-focus application where the primary requirement is to evaluate the relative sharpnesses of a sequence images of the same scene being focused. Our method is in the DCT domain. Compared with other transform algorithms such as FFT or DWT, DCT

has an important advantage is that DCT can be computed efficiently by using optimized DCT-specific platforms [29, 30] and fast computation algorithms [31]. Another advantage is many video encoding algorithms are based on block-based DCT data [32, 33]. This allows us to exploit the already available DCT coefficients and may reach sharpness metrics of high efficiency.

### 3.1 A Reorganized DCT Representation

DCT is an algorithm that transforms image data of spatial-domain into frequency-domain. Let $f(x, y)$ denotes the spatial pixel value at $(x, y)$ of an image with size $M \times N$, $F(i, j)$ denotes the corresponding DCT frequency components, the mapping between $f(x, y)$ and $F(i, j)$ is:

$$F(i,j) = \sum_{(x,y)} f(x,y) C_{ij}(x,y;M,N) \tag{1}$$

where $C_{ij}$ are orthogonal 2D basis functions, defined as

$$C_{ij} = c_i(x;M)c_j(y;N) \tag{2}$$

where

$$c_\varphi(z;A) = \alpha(\varphi;A)cos(\frac{\pi\varphi(2z+1)}{2A}) \tag{3}$$

$$\alpha(\varphi;A) = \begin{cases} \frac{1}{\sqrt{A}} \text{ if } \varphi = 0; \\ \sqrt{\frac{2}{A}} \text{ otherwise.} \end{cases} \tag{4}$$

For sharpness measure, we are interested in using $8 \times 8$ DCT which carries the transform on $8 \times 8$ pixel blocks. Several efficient algorithms and hardware implementation solutions exist for this block based DCT [6]. The operation of $8 \times 8$ DCT would result in a series of 64 coefficients$\{F(i, j)|i = 0, 1, \cdots, 7, j = 0, 1, \cdots, 7\}$, where $F(0, 0)$ is the DC coefficient, and the others are AC coefficients. Each of these coefficients represents a particular spatial frequency.

A typical image is consisted of a set of smooth regions delimited by edge discontinuities. After applied block-based DCT operation, the image energy of smooth regions is compacted into the DC coeffiients together with a few high-frequency AC coefficients, while the energy of edges is compacted into a small number of high-frequency AC coefficients [34, 33]. This energy compaction property of DCT allows us to select a set of high-frequency components that are related to the edges in spatial domain for measuring sharpness.We exploit a reorganization strategy of DCT coefficients [32, 34] for finding the most suitable components that have high effect on focus measure. In this reorganization, each $8 \times 8$ block is taken as a three scale tree of coefficients with 10 subbands decomposition, as shown in Fig 1(a). After that, the coefficients of the same subbands for all blocks are grouped together and put onto their corresponding positions (Fig. 1(b)). Fig. 1(c) shows an example of the reorganization representation of

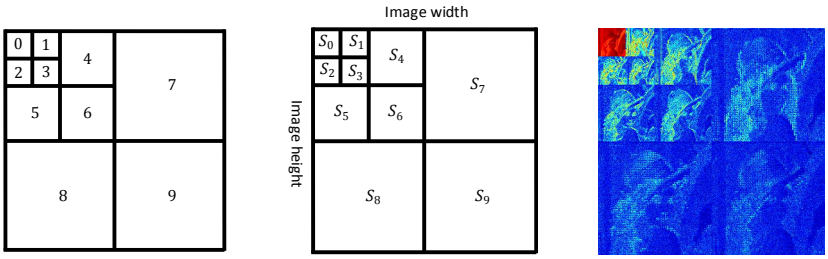


(a) (b) (c)

**Fig. 1.** Reorganization strategy of DCT coefficients. (a) Each $8 \times 8$ block is taken as three-scale tree with ten-subband decomposition; (b) The reorganization representation for an image where coefficients of the same subbands for all $8 \times 8$ blocks are grouped together and put onto their corresponding positions; (c) reorganization result of Lena image;

| | | | | |
|---|---|---|---|---|
| Subband 4 | $F(0,2)$ | $F(0,3)$ | $F(1,2)$ | $F(1,3)$ |
| | **0.5348** | 0.1576 | 0.2070 | 0.1006 |
| Subband 5 | $F(2,0)$ | $F(2,1)$ | $F(3,0)$ | $F(3,1)$ |
| | **0.4706** | 0.3001 | 0.1159 | 0.1159 |
| Subband 6 | $F(2,2)$ | $F(2,3)$ | $F(3,2)$ | $F(3,3)$ |
| | **0.4806** | 0.2355 | 0.1674 | 0.1165 |

**Table 1.** Enery ratios of each coefficient to the total four coefficients in each subband of Lena image. Each ratio is computed using energy of the corresponding coefficients collected from all blocks.

one image. It is seen that this form of reorganization of block-based DCT coefficients has structural similar characteristics to the three-scale multiresolution decomposition of discrete wavelet transform [35]. For example, the DCT subbands $S_7$, $S_8$ and $S_9$ correspond to the level-1 HL, LH and HH subbands of DWT separately.

### 3.2 The Metric

Our sharpness measures exploit the structural similarities between the subbands of multi-scale DWT and the reorganized subbands of block-based DCT. For three-level DWT data, low frequency components increase with the level of subbands, where the subbands of level-1 and level-2 are dominated by high and middle frequency coefficients. Since the subbands $\{S_i|i = 7, 8, 9\}$ and $\{S_i|i = 4, 5, 6\}$ of reorganized DCT correspond to the level-1 and level-2 subbands of DWT respectively, it is reasonable to calculate the sharpness using the components in these DCT subbands regions.

To select the optimum coefficient components that have high discrimination power, we analyze and compare the different effects of using middle and high

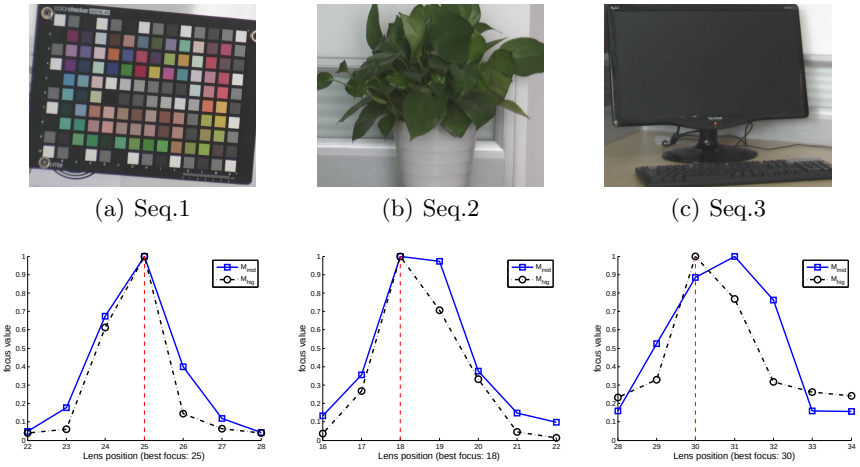


(a) Seq.1 (b) Seq.2 (c) Seq.3

(d) Seq.1 (e) Seq.2 (f) Seq.3

**Fig. 2.** Comparison of middle-frequency and high-frequency based sharpness measure. Above: best-focus images of three sequences taken with different subjects; Below: sharpness or focus values of few neighbor positions around the best focused position are shown.

frequencies on measuring sharpness. According to the structural similarities between reorganized DCT and DWT coefficients, we select middle frequencies from subbands (4, 5, 6) and high frequencies from subbands (7, 8, 9) for each $8 \times 8$ DCT block. Taking signal power of all coefficients in the corresponding subbands to measure sharpness is one possible way, but it would certainly need high computational cost. Since the histograms of corresponding coefficients collected from all blocks shows that the signal energy is usually concentrated in the lower frequency bands [36], we use the coefficients centralized in upper left corner of each subband. Table. 1 gives the energy ratios of each coefficient to all coefficients in the corresponding subbands of Lena image. These ratios are computed using all block data. It is seen that about half of the energy associated with subbands 4, 5 and 6 is taken up by the corresponding upper left coefficients. Hence, we choose the three upper left corner coefficients for the case of middle frequency based metric, *i.e.*, $F(0,2)$ of subband 4, $F(2,0)$ of subband 5 and $F(2,2)$ of subband 6. We define the middle-frequency sharpness metric of single block as follows:

$$M_{mid} = |F(0,2)|^2 + |F(2,0)|^2 + |F(2,2)|^2 \tag{5}$$

The high frequency based metric is defined in a similar way. In the three scale tree decomposition (Fig. 1(a)), each coefficient of subbands 4, 5, and 6 is associated with four children in subbands 7, 8 and 9 respectively. For instance, coefficients $F(0,4)$, $F(0,5)$, $F(1,4)$ and $F(1,5)$ are the four children of the parent coefficient $F(0,2)$. It can be found that much of the energy of subbands 7, 8, and 9 is also concentrated in the corresponding four children. We define the

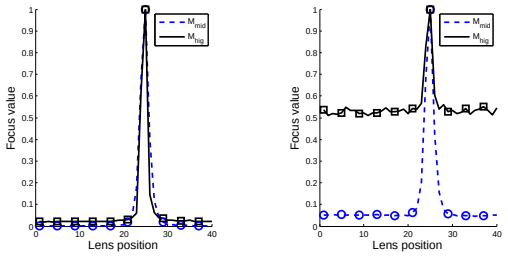


**Fig. 3.** Sharpness measures on the synthetic noisy image sequence. (a-b) the focus curves on Seq.1 without (a) and with white Gaussian noise (b); Note that each point of the focus curves is normalized by the corresponding maximum sharpness.

high frequency metric as follows:

$$M_{hig} = \sum_{i=0}^{1}\sum_{j=4}^{5}|F(i,j)|^2 + \sum_{i=4}^{5}\sum_{j=0}^{1}|F(i,j)|^2 + \sum_{i=4}^{5}\sum_{j=4}^{5}|F(i,j)|^2 \tag{6}$$

Fig. 2 gives the focus curves of the two measures on three sequences. The average sharpness of all blocks are taken into account for focus evaluation. It is seen that both measures have a peak at the best focused position, but $M_{hig}$ gives sharper focus curves. For Seq.3 only $M_{hig}$ gives sharpest value at the correct focus position. These figures indicate that $M_{hig}$ is more sensitive to best focused position. Fig. 3 plots focus curves of the two measures for the images with and without noise added, where the synthetic noisy image is generated by adding Gaussian noise with standard deviation 20 to Seq.1. We can see that though both measures produce maxima values at the best focused position, $M_{mid}$ shows more robust performance as its focus curve is less effected by noise, while $M_{hig}$ has smaller dynamic sharpness range around the peak. We may conclude that using high frequencies for focus measuring, *e.g.*, $M_{hig}$, would have higher discrimination power as they are more sensitive to the best-focus position, but may be effected by noise. On the contrast, the middle frequency based measures like $M_{mid}$ shows very strong robustness of anti-noise but may lack of discriminativity in ambiguous cases. Our proposed relative sharpness metric $M_{reodct}$ combines both middle and high frequencies in a linear form defined as follows:

$$M_{reodct} = \lambda M_{mid} + M^*_{hig} \tag{7}$$

where $\lambda$ is a factor that balances the effect of both measures $M_{mid}$ and $M^*_{hig}$. $M^*_{hig}$ is a variant of $M_{hig}$ and is defined as:

$$\begin{aligned} M^*_{hig} = {} & |F(0,4)|^2 + |F(0,5)|^2 + |F(1,4)|^2 \\ & + |F(4,0)|^2 + |F(4,1)|^2 + |F(5,0)|^2 \\ & + |F(4,4)|^2 + |F(4,5)|^2 + |F(5,4)|^2 \end{aligned} \tag{8}$$

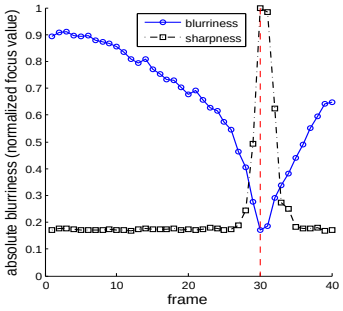


**Fig. 4.** Blurriness and focus value curves of one sample sequence.

where three coefficient components, *i.e.*, $F(1,5)$, $F(5,1)$ and $F(5,5)$ are removed from the part of $M_{hig}$. We find this in addition to being less computation consuming but almost reduces no performance of the measure.

### 3.3 Sharpness Detection Ability (SDA) Measure

A good sharpness measure should decrease with an increasing blurring. Higher measure difference between the consecutive values indicates stronger discrimination ability. Let $M_t$ denotes the normalized focus measure of image frame $t$, $\sigma_t$ is the corresponding Gaussian blur standard deviation. Give measures on frames $t = 1, \cdots, T$, we define a new metric named Sharpness Detection Ability measure (SDA) to quantify the sharpness functions. SDA is defined as a psychometric function [37] which can be modeled as follows:

$$SDA = \frac{1}{T}\sum_{t=1}^{T} 1 - exp\Big( - \Big| \frac{M_{t+1} - M_t}{\sigma_{t+1} - \sigma_t} \Big|^{\frac{1}{\sigma_{t+1}}} \Big) \tag{9}$$

SDA is designed to produce higher value on larger sharpness differences with smaller blur deviation between consecutive images. This means it is a good indicator of sensitivity to best focus. Additionally, if the consecutive sharpness measure differences change inverse proportionally with the corresponding deviation differences, the metric would produce larger value which indicates better sharpness discrimination power.

## 4 The Proposed Absolute Sharpness Metric

### 4.1 Our Motivation

One problem of the initialization stage in autofocusing is to set the size of focusing-step properly. A smaller focusing-step size should be used when the starting image is sharper, and a larger step should be used when the image is blurred. This requires to know the absolute sharpness or blurriness of the starting

image. Another problem is to decide which direction to move the focus motor. Searching in a wrong direction would causes slow focusing which is a bad visual experience. Since the arbitrary starting position may be severely blurred or very close to best-focus position, it is difficult to successfully judge the direction efficiently for all cases.

Fig. 4 shows blurriness (*i.e.*, the absolute sharpness) and focus value curves for one focusing sequence. It is seen that the absolute sharpness curve monotonously decreases with the increase of focus value, showing high discriminative power in distinguishing blurriness even in the area where the focus value curve is very flat. This motivates us to exploit both absolute sharpness and focus value (*i.e.*, the relative sharpness) for solving the aforementioned problems. Using the relative sharpness measures of autofocusing to decide the absolute blurriness of image would meet problems. This is because that they are highly dependent on image content, and they provide relative sharpness values that are meaningful only for an entire focusing sequence captured at the same scene. Most existing absolute sharpness/blurriness estimation algorithms [12, 11, 27] are proposed for image quality assessment. They are not suitable for our task due to their high computational complexity.

### 4.2 The Algorithm

This algorithm is inspired by the work [27] that uses Harr wavelet transform (HWT) for blur detection. In this work, image edges are classified into four types: Dirac-Structure, Astep-Structure, Gstep-Structure, and Roof-Structure. When blur happens both Dirac-Structure and Astep-Structure edges will disappear, and Gstep-Structure as well as Roof-Structure tend to lose their sharpness. The algorithm performs edge detection by finding the local maxima on three-scale HWT of the image, and counts the numbers of each edge type according to a set of rules. As a result, the blur degree is calculated using the ratio of the number of Roof-Structure and Gstep-Structure edges that lost their sharpness to the total number of Roof-Structure and Gstep-Structure edges.

The above blur detection method works effectively for out-of-focus or linear motion blur. However, the use of HWT that consumes much extra computational resources would not be suitable for the auto-focus application where the main processing is in the DCT domain. Moreover, we find that the algorithm is fairly sensitive to noise. In our method, blur estimation is performed in the DCT domain where we exploit the reorganized DCT representation described in Sect. 3.1. An energy map for each level $i$ of the three-level ($i = 1, 2, 3$) DCT coefficients is firstly constructed as follows:

$$E_i(k,l) = \sqrt{\big(S_{i1}(k,l)\big)^2 + \big(S_{i2}(k,l)\big)^2} \tag{10}$$

where $\{S_{ij}|j = 1, 2, 3\}$ with $S_{ij} = S_{(3-i)\times 3+j}$ denote the subbands associated with the level $i$ decomposition in the reorganized DCT representation, as illustrated in Fig. 1(b). In Equ. 10, the coefficients of subbands $S_3, S_6, S_9$ are neglected for energy calculation. This is because that these subbands consist

**Algorithm 1:** Absolute sharpness or blurriness estimation using the reorganized block DCT

(1). Compute $8 \times 8$ DCT of the image of interest, construct energy maps $E_i$ using Equ. 10 for each scale of DCT coefficients in the reorganized representation.
(2). Find the local maxima of each block for every energy map to obtain three edge maps $EM_i$.
(3). Set $N_{rg} \leftarrow 0$, $N_{blur} \leftarrow 0$; **for** *every point* $(k, l)$ **do**
  **if** $EM_1(k,l) \geq T_1 || EM_2(k,l) \geq T_1 || EM_3(k,l) \geq T_1$ **then**
    **if** $EM_1(k,l) \leq EM_2(k,l) \leq EM_3(k,l) ||$
    $EM_2(k,l) \geq EM_1(k,l) \&\& \; EM_2(k,l) \geq EM_3(k,l)$ **then**
      $N_{rg} \leftarrow N_{rg} + 1$;
      **if** $EM_2(k,l) \leq T_2$ **then**
        $N_{blur} \leftarrow N_{blur} + 1$;
(4). Compute blurriness $B = \frac{N_{blur}}{N_{rg}}$.

of relative higher frequency components, of which the energy is more easily affected by noise. After that, three edge maps $\{EM_i | i = 1, 2, 3\}$ of the same size are extracted by finding the local maxima of every block in each energy map. The block size of $E_i$ is $2^{a-i} \times 2^{a-i}$, where $a$ is usually set to 3 or 4.

Considering that the energy of DCT coefficient tends to centralize in upper left corner of each subband, we can construct $E_1$ by only using the upper left coefficients of each block. For instance, $\{F_{i,j} | i = 4, 5; j = 0, 1;\}$ and $\{F_{i,j} | i = 0, 1; j = 4, 5;\}$ of each $8 \times 8$ block are used to construct $E_1$ for the case when $a = 3$. Accordingly the maxima energy of the 4 coefficients of each block are then taken as the local maxima for building edge map $EM_1$. This would significantly increase the computational efficiency.

Two threshold parameters $T_i (i = 1, 2)$ $(T_2 \geq T_1)$ are used in our algorithm. $T_1$ is used for detecting edge points, and $T_2$ is for judging edge points that lose sharpness. For any Gstep-Structure or Roof-Structure edge point $(k, l)$, our algorithm decides whether this point is blurred by: $EM_2(k, l) < T_2$. Since the edge map $EM_1$ is based on high frequency coefficients, it is more sensitive to noise. By contrast, the use of edge map $EM_2$ for finding blurred points leads to strong anti-noise ability. The presented method is summarized in Algorithm 1.

## 5 Experiments

We first evaluate our proposed relative sharpness metric on public available dataset. A total of five spatial-domain measures and four DCT-based measures are compared with the proposed metric $M_{reodct}$. The spatial-domain measures include the Tenengrad or Sobe function $M_{sob}$, the Squared gradient $M_{sqg}$, the sum of differences across rows and columns $M_{smd}$, the sum of Laplacians $M_{sml}$, and the energy of Laplacians $M_{eol}$. Definitions of these measures are not given here as they can be explicitly found in several related works [3, 7, 9]. The four DCT-based methods include the Bayes spectral entropy based measure $M_{bsedct}$ [6],

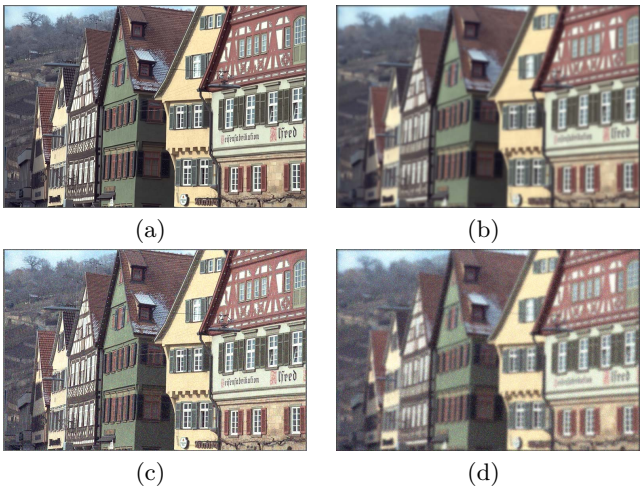

**Fig. 5.** Above row: two sample Gaussian blur images of the same scene from the LIVE dataset [14], (a) blur deviation $\sigma = 0$, (b) $\sigma = 2.624972$; Below row: white noise is added to the corresponding images (c-d), with noise deviation $\sigma_{noise} = 30$.

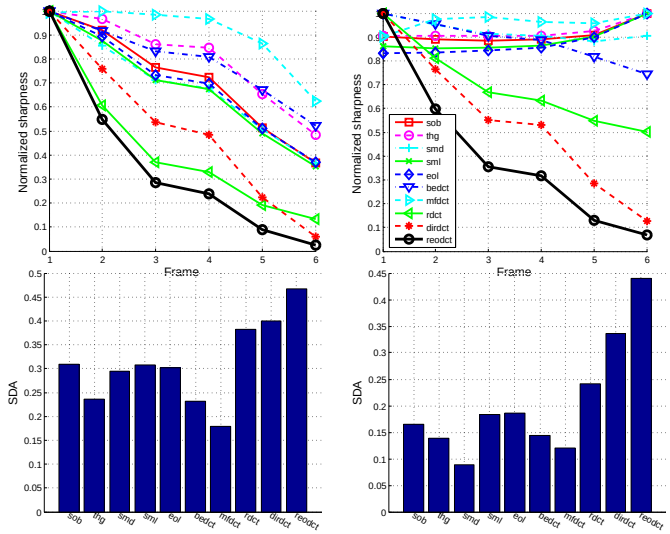


**Fig. 6.** Above row: sharpness measures on "building" sequence without (a) and with noise (b); Below row: the corresponding SDA evaluations.

| | $\sigma_{noise} = 30$ | | | | | |
|---|---|---|---|---|---|---|
| Measure | $M_{sob}$ | $M_{sml}$ | $M_{eol}$ | $M_{bedct}$ | $M_{dirdct}$ | $M_{reodct}$ |
| coinsinfountain | 0.1018 | 0.0920 | 0.0911 | 0.2169 | 0.3484 | **0.3640** |
| ocean | 0.1018 | 0.0920 | 0.0911 | 0.2169 | 0.3484 | **0.3640** |
| statue | 0.1516 | 0.1455 | 0.1455 | 0.2023 | **0.3437** | 0.3213 |
| dancers | 0.1976 | 0.2099 | 0.2077 | 0.3134 | 0.3619 | **0.4145** |
| paintedhouse | 0.1599 | 0.1562 | 0.1562 | 0.1956 | 0.3819 | **0.4001** |
| stream | 0.1174 | 0.1160 | 0.1105 | 0.3160 | 0.3158 | **0.4674** |
| bikes | 0.2223 | 0.2435 | 0.2409 | 0.3177 | 0.3569 | **0.4316** |
| flowersoih35 | 0.1972 | 0.1910 | 0.1859 | 0.3064 | 0.3224 | **0.4516** |
| parrots | 0.1592 | 0.1655 | 0.1656 | 0.2688 | **0.3532** | 0.3511 |
| studentsculpture | 0.1157 | 0.1257 | 0.1282 | 0.2705 | 0.3694 | **0.4520** |
| building2 | 0.0862 | 0.0795 | 0.0702 | 0.3263 | 0.3916 | **0.4919** |
| plane | 0.2178 | 0.2216 | 0.2222 | 0.3145 | 0.3430 | **0.4040** |
| woman | 0.1287 | 0.1351 | 0.1297 | 0.2369 | 0.3641 | **0.3648** |
| house | 0.2271 | 0.2233 | 0.2214 | 0.2169 | 0.3960 | **0.4116** |
| rapids | 0.1550 | 0.1563 | 0.1523 | 0.3385 | 0.3688 | **0.4469** |
| womanhat | 0.0772 | 0.0752 | 0.0749 | 0.1456 | 0.2879 | **0.3047** |
| caps | 0.2155 | 0.2171 | 0.2177 | 0.2011 | 0.3405 | **0.3568** |
| lighthouse | 0.1903 | 0.1797 | 0.1770 | 0.2853 | 0.4055 | **0.4604** |
| sailing1 | 0.1464 | 0.1476 | 0.1449 | 0.2716 | 0.3987 | **0.4691** |
| carnivaldolls | 0.1046 | 0.0987 | 0.0968 | 0.2339 | 0.3366 | **0.3626** |
| lighthouse2 | 0.0875 | 0.1044 | 0.1075 | 0.2426 | 0.3367 | **0.3884** |
| sailing2 | 0.1556 | 0.1618 | 0.1643 | 0.1867 | 0.3989 | **0.4111** |
| cemetry | 0.1126 | 0.1312 | 0.1339 | 0.3070 | 0.3644 | **0.4476** |
| manfishing | 0.1815 | 0.1707 | 0.1610 | 0.2140 | 0.3324 | **0.3967** |
| sailing3 | 0.1267 | 0.1261 | 0.1253 | 0.1415 | 0.2561 | **0.2681** |
| churchandcapitol | 0.1674 | 0.1884 | 0.1956 | 0.3430 | 0.4112 | **0.4512** |
| monarch | 0.3166 | 0.3136 | 0.3166 | 0.3642 | 0.3881 | **0.4181** |
| sailing4 | 0.2495 | 0.2413 | 0.2374 | 0.3545 | 0.4010 | **0.4598** |

**Table 2.** SDA accuracy between different sharpness measures on LIVE Gaussian blur sequences with sythetic noises.

the middle frequency component based measure $M_{mfdct}$ [7], the ratio of AC and DC energy based measure $M_{rdct}$ [8], and the block direction information based measure $M_{dirdct}$ [9]. The public available dataset LIVE [14] is used for the comparison experiments. LIVE provides 145 Gaussian blur images which are created from 29 input images. Fig. 5 shows example Gaussian blur images of LIVE.

Fig. 6(a) plots the sharpness evaluation results on one blur image sequence named "buildings" of LIVE (Fig. 6). Fig. 6(c) gives the corresponding evaluations of SDA. The DCT based sharpness measures like $M_{rdct}$, $M_{dirdct}$ and the proposed one show relative better performance than all spatial-domain functions. To test noise sensitivity of the proposed measure, white Gaussian noise of standard deviation $\sigma_{noise}$ is added to the blur images, and the 10 sharpness measures are tested again. Fig. 6(b) and 6(d) gives the results on the noised "buildings" sequence. We can see all measures except of $M_{reodct}$ and $M_{dirdct}$ are

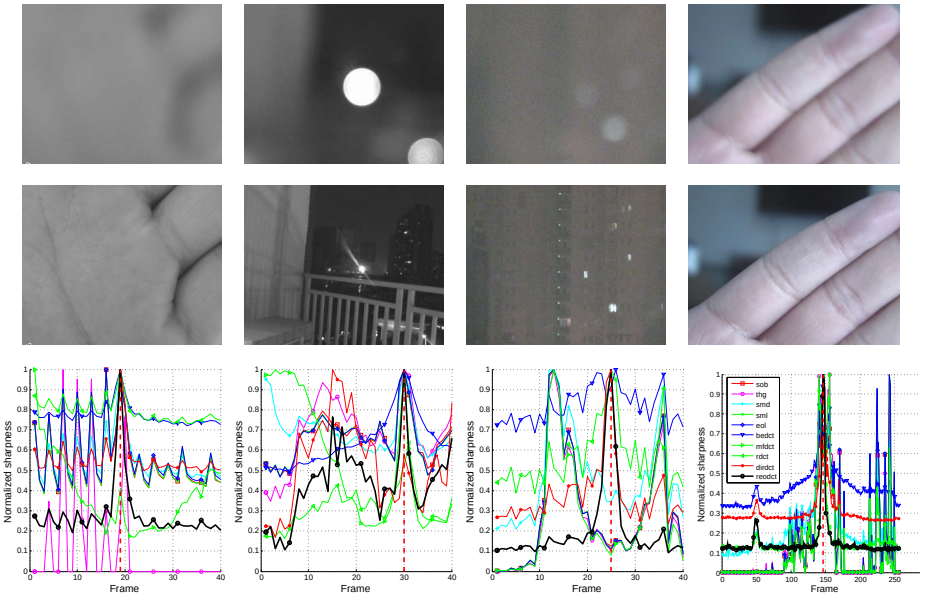


**Fig. 7.** From left to right: sharpness measuring on example sequences of scenes with low contrast ("Hand"), strong lighting ("LightBeam"), high noise ("NightBuilding") and moving objects ("MovingFingers").

seriously affected by noise. Table 2 gives SDA evaluations of the 6 measures including $M_{sob}$, $M_{sml}$, $M_{eol}$, $M_{rdct}$, $M_{dirdct}$ and $M_{reodct}$ on the 29 LIVE Gaussian image sequences with synthetic noise. It is found that $M_{reodct}$ shows very robust performance and outperforms other measures both in accuracy and robustness.

The proposed sharpness measure is also tested on four real focusing sequences, which are labeled as "Hand", "LightBeam", "NightBuilding" and "MovingFingers". As shown in Fig. 7, the Hand sequence is poor in contrast, the LightBeam has strong lighting distortions, the NightBuilding is captured at low illumination, and the MovingFingers is a sequence of moving subject. For all evaluation, the center window of size $\frac{1}{3}w \times \frac{1}{3}h$ ($w$ and $h$ denote the image width and height separately) is taken as the area for sharpness calculation. For the Hand sequence, we can see from the focus curves that only $M_{reodct}$ gives largest sharpness dynamic range and correct position of best focus. In sequence LightBeam, the factors such as halo edges and illumination changes would largely affect the sharpness measure. Multiple peaks and many fluctuations may exist, as seen from the focus curves. The results show that the proposed measure $M_{reodct}$ is able to give the correct maximum measure for this complex case. For sequence NightBuilding which is polluted by noise due to the low illumination, $M_{reodct}$ shows the best performance of anti-noise. It also produces stable and reliable estimations when the subject is moving, as can be seen from the result of the sequence MovingFingers.

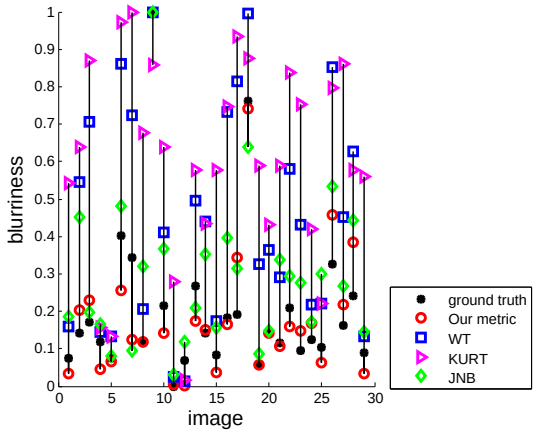


**Fig. 8.** Blur estimation for sample Gaussian blurred images of LIVE dataset, of which the blurred image set is obtained by filtering 29 input images with different content using Gaussian kernel of different standard deviation $\sigma$. For all images, our algorithm uses $T_1 = 5$, $T_2 = 10$, while other algorithms use the optimal parameters as suggested. The normalized $\sigma$ is taken as the ground truth of blurriness.

We have tested the proposed no-reference metric of absolute sharpness on the Gaussian blur sequence of the public LIVE dataset. From the given 145 Gaussian blur images, we select 29 blurred images that have different blur $\sigma$ and image contents. Three commonly used metrics are chosen for performance comparison: the wavelet transform method (WT) [27], the kurtosis method (KURT) [26], and the just noticeable blur method (JNB) [12]. The parameters of each algorithm are set according to the optimal suggestions described in the relevant work. Fig. 8 gives the result of the four metrics for judging blurred points. It is seen that our metric outperforms other methods both in robustness and accuracy.

## 6 Conclusion

In this work, we propose two sharpness metrics by exploiting a reorganized DCT representation. The first metric selects the most suitable components that have high effect on sharpness measuring. This metric has high discrimination power even for high noisy and low-contrast images. We have used it for auto-focus application where it shows super sensitive to the best-focus position and could predict stable sharpness measures for various subjects and scenes with different lighting and noise conditions. We also present an efficient DCT-based absolute sharpness metric. This metric exploits the same framework of the reorganized DCT representation. It correlates well with perceived sharpness and is efficient in sharpness measurement for images with different contents. We demonstrate the performance of our metrics by comparing them against several most commonly used metrics both on public and the captured out-of-focus sequences.

## References


1. Ciancio, A., da Costa, A.L.N.T., da Silva, E.A.B.: No-reference blur assessment of digital pictures based on multifeature classifiers. IEEE Transactions on Image Processing **20** (2011) 64–75
2. Vu, C.T., Phan, T.D., Chandler, D.M.: S3: A spectral and spatial measure of local perceived sharpness in natural images. IEEE Transactions on Image Processing **21** (2011) 934–945
3. Santos, A., Solorzano, C.O.D., Vaquero, J.J., Pena, J.M., Malpica, N., Pozo, F.D.: Evaluation of autofocus functions in molecular cytogenetic analysis. Journal of Microscopy **188** (1997) 264–272
4. Yousefi, S., Rahman, M., Kehtarnavaz, N.: A new auto-focus sharpness function for digital and smart-phone cameras. IEEE Transactions on Consumer Electronics **57** (2011) 1003–1009
5. Choi, J., Kang, H., Lee, C.M., Kang, M.G.: Noise insensitive focus value operator for digital imaging systems. IEEE Transactions on Consumer Electronics **56** (2010) 312–316
6. Kristan, M., Pers, J., Perse, M., Kovacic, S.: A bayes-spectral-entropy-based measure of camera focus using a discrete cosine transform. Pattern Recognition Letters **27** (2006) 1431–1439
7. Lee, S.Y., Kumar, Y., man Cho, J., Lee, S.W., Kim, S.W.: Enhanced autofocus algorithm using robust focus measure and fuzzy reasoning. IEEE Transactions on Circuits and Systems for Video Technology **18** (2008) 1237–1246
8. Shen, C.H., Chen, H.H.: Robust focus measure for low-contrast images. In: IEEE International Conference on Consumer Electronics. (2006)
9. Jeon, J., Lee, J., Paik, J.: Robust focus measure for unsupervised auto-focusing based on optimum discrete cosine transform coefficients. IEEE Transactions on Consumer Electronics **57** (2011) 1–5
10. Lee, M.E., Chen, C.F., Lin, T.N., Chen, C.N.: The application of discrete cosine transform combined with the nonlinear regression routine on optical auto-focusing. In: IEEE International Conference on Consumer Electronics. (2009)
11. Marichal, X., Ma, W.Y., Zhang, H.: Blur determination in the compressed domain using dct information. In: IEEE International Conference on Image Processing. (1999)
12. Ferzli, R., Karam, L.J.: A no-reference objective image sharpness metric based on the notion of just noticeable blur. IEEE Transactions on image processing **18** (2009) 717–728
13. Shen, J., Li, Q., Erlebacher, G.: Hybrid no-reference natural image quality assessment of noisy, blurry, jpeg2000, and jpeg images. IEEE Transactions on Image Processing **20** (2011) 2089–2098
14. Sheikh, H.R., Wang, Z., Cormack, L., Bovik, A.C.: Live image qaulity assessment database release 2. (`http://live.ece.utexas.edu/research/quality.`)
15. Zhang, Y., Zhang, Y., Wen, C.: A new focus measure method using moments. Image and Vision Computing **18** (2000) 959–965
16. Kautsky, J., Flusser, J., Zitova, B., Simberova, S.: A new wavelet-based measure of image focus. Pattern Recognition Letters **23** (2002) 1785–1794
17. Yang, G., Nelson, B.J.: Wavelet-based autofocusing and unsupervised segmentation of microscopic images. In: IEEE International Conference on Intelligent Robots and Systems. (2003)

18. Horn, B.K.P.: Focusing. Technical report, Massachusetts Institute of Technology (1968)
19. Choi, K.S., Lee, J.S., Ko, S.J.: New autofocusing technique using the frequency selective weighted median filter for video cameras. IEEE Transactions on Consumer Electronics **45** (1999) 820–827
20. Chen, C.Y., Hwang, R.C., ju Chen, Y.: A passive auto-focus camera control system. Applied Soft Computing **10** (2010) 296–303
21. Marziliano, P., Dufaux, F., Winkler, S., Ebrahimi, T.: A no-reference perceptual blur metric. In: IEEE International Conference on Image Processing. (2002)
22. Marziliano, P., Dufaux, F., Winkler, S., Ebrahimi, T.: Perceptual blur and ringing metrics application to jpeg2000. Signal Processing: Image Communication **19** (2004) 163–172
23. Narvekar, N.D., Karam, L.J.: A no-reference image blur metric based on the cumulative probability of blur detection. IEEE Transactions on Image Processing **20** (2011) 2678–2683
24. Sadaka, N.G., Karam, L.J., Ferzli, R., Abousleman, G.P.: A no-reference perceptual image sharpness metric based on saliency-weighted foveal pooling. In: IEEE International Conference on Image Processing. (2008)
25. Wee, C.Y., Paramesran, R.: Image sharpness measure using eigevalues. In: 9th international conference on signal processing. (2008)
26. Caviedes, J., Oberti, F.: A new sharpness metric based on local kurtosis, edge and energy information. Signal Processing: Image Communication **19** (2004) 147–161
27. Tong, H., Li, M., Zhang, H., Zhang, C.: Blur detection for digital images using wavelet transform. In: IEEE International Conference on Multimedia and Expo. (2004)
28. Shaked, D., Tastl, I.: Sharpness measure: Towards automatic image enhancement. In: IEEE International Conference on Image Processing. (2005)
29. Balam, S., Schonfeld, D.: Associative processors for video coding applications. IEEE Trans. Circuits Syst. Video Technol. **16** (2006) 241–250
30. Huan, J., Parris, M., Lee, J., DeMara, R.F.: Scalable fpga-based architecture for dct computation using dynamic partial reconfiguration. ACM Trans. Embedded Comput. Syst. **9** (2009) 1–18
31. Cho, N.I., Lee, S.U.: Fast algorithm and implementation of 2d discrete cosine transform. IEEE Trans. Circuits Syst. **38** (1991) 297–305
32. Xiong, Z., Guleryuz, O., Orchard, M.T.: A dct-based embedded image coder. Signal Processing Letters **3** (1996) 289–290
33. Ma, L., Li, S., Zhang, F., Ngan, K.N.: Reduced-reference image quality assessment using reorganized dct-based image representation. IEEE Transactions on Multimedia **13** (2011) 824–829
34. Zhao, D., Gao, W., Chan, Y.K.: Morphological representation of dct coefficients for image compression. IEEE Transactions on Circuits and Systems for Video Technology **12** (2002) 819–823
35. Mallat, S.: A theory for multiresolution signal decomposition: The wavelet representation. IEEE Transactions on Pattern Analysis and Machine Intelligence **11** (1989) 674–693
36. Lam, E.Y., Goodman, J.W.: A mathematical analysis of the dct coefficient distributions for images. IEEE Transactions on Image Processing **9** (2000) 1661–1666
37. Robson, J.G., Graham, N.: Probability summation and regional variation in contrast sensitivity across the visual field. Vision Research **21** (1981) 409–418